HnRNP-L regulated circCSPP1/miR-520h/EGR1 axis modulates autophagy and promotes progression in prostate cancer

Jianming Lu
Zhujiang Hospital
Chuanfan Zhong
Zhujiang Hospital
Fangpeng Shu
Guangzhou Women and Children's Medical Center
Daojun Lv
Guangzhou Medical College First Affiliated Hospital
Zezhen Liu
Guangzhou Medical College First Affiliated Hospital
Xiao Tan
Southwest Medical University
Shuo Wang
Zhujiang Hospital
Kaihui Wu
Zhujiang Hospital
Taowei Yang
Zhujiang Hospital
Weibo Zhong
Zhujiang Hospital
Bin Wang
Guangzhou Medical University Affiliated Cancer Hospital
Yanfei Chen
Guangzhou Medical University Affiliated Cancer Hospital
Yuehan Li
University of Southern California
Zhenyu Jia
University of California Riverside
Yaguan Zou
Southern Medical University Nanfang Hospital
Weide Zhong

Southern Medical University Nanfang Hospital
Xiangming Mao (mxm631221@126.com)
Southern Medical University

Research

Keywords: prostate cancer, circCSPP1, microRNA-520h, EGR1, autophagy, progression

Posted Date: January 19th, 2021

DOI: https://doi.org/10.21203/rs.3.rs-147854/v1

Version of Record: A version of this preprint was published at Molecular Therapy - Nucleic Acids on December 1st, 2021. See the published version at https://doi.org/10.1016/j.omtn.2021.10.006.

Abstract

Background

The circRNAs, a new subclass of non-coding RNAs that are catalyzed by RNA-binding proteins (RBPs), have been reported to be associated with the progression of multiple types of cancers. We previously discovered that heterogeneous nuclear ribonucleoprotein L (HnRNP-L), a multi-functional RNA RBP, is associated with pro-proliferation and anti-apoptosis activities in prostate tumor cells. In this study, we aim to establish the biological relevance of circCSPP1 (a newly discovered signature circRNA in prostate cancer) and HnRNP-L to prostate cancer (PCa) progression.

Methods

The specific expression level of circCSPP1 (not confounded by the linear-CSPP1) in PCa was investigated and analyzed based on the publicly available datasets, and was quantified *in vitro* or in *vivo* using FISH and RT-qPCR in the current study. The RT-qPCR, RNA immunoprecipitation (RIP) and mini-gene system were utilized to confirm that the expression of circCSPP1 was determined by HnRNP-L. We verified the autophagy-induced tumor-promoting effect of circCSPP1 in PCa through a series of gain-of-function and loss-of-function experiments *in vitro* or in *vivo*. The western blot, confocal microscope and transmission electron microscope (TEM) were employed in autophagy assays. Advanced bioinformatics analyses, dual-luciferase reporter assay, FISH and AGO2 RIP were applied to identify the endogenous RNA network involving circCSPP1/miR-520 h/EGR1 axis in PCa, which promote PCa progression through regulating autophagy activities.

Results

First, we demonstrated that circCSPP1 expression was higher in PCa tissues than in benign tissues, and higher in PCa cells than in the benign cells. Then, the *in vitro* gain- and loss-of-function experiments showed that the circCSPP1 expression in PCa cells was regulated by HnRNP-L, and the increased circCSPP1 significantly induced autophagy which led to an enhanced potential in proliferation, migration and invasion of PCa cells. These results were consistent with the *in vivo* experiment where increased circCSPP1 was associated with higher growth rate in grafted tumors. Finally, we demonstrated the potential competing endogenous RNA network, involving circCSPP1, miR-520 h, and EGR1, in PCa cells, which may play an important role in PCa progression.

Conclusions

Our study indicated that the increase in circCSPP1 in PCa, which may be catalyzed by HnRNP-L, can induce cellular autophagy through the CircCSPP1-miR-520 h-EGR1 axis, leading to the progression of

prostate tumor. This newly discovered circRNA biomarker may be used for clinical prognosis of PCa as well as for development of novel therapy plans.

Background

Prostate cancer remains the second leading cause of cancer death in American men, only behind lung cancer [1]. The incidence and mortality of prostate cancer are both rising steadily in multiple countries [2]. Many molecular mechanisms have been proposed for formation and progression of prostate cancer, including DNA somatic mutations, harmful gene fusions, irregular methylation, and aberrant RNA splicing [3, 4]. Moreover, a recent study showed that knockout of Atg7 (a key autophagic regulator) inhibited prostate cancer progression in castrate-resistant or castrate-sensitivity prostate cancer, suggesting that dysfunctional autophagy may be also associated with prostate cancer progression [5]. However, the current knowledge of the disease is still limited, which can barely account for the heterogeneous nature of prostate tumors. New insights at molecular levels and organelle levels are needed to improve our understanding of this complex disease, and to develop novel tools for diagnosis and prognosis, and new strategies for personalized treatment [6].

The majority of the human genome consists of noncoding DNAs, many of which are transcribed to non-coding RNAs, including microRNAs(miRNAs) and long non-coding RNAs (lncRNAs) [7]. Research has shown that non-coding RNAs may play important roles in the development and progression of prostate cancer [8]. Recently, mounting attention has been brought to circRNAs – a newly uncovered type of non-coding RNAs which may also play a vital role in tumorigenesis and progression [9]. Catalyzed by certain RNA-binding proteins (RBPs), precursor RNA molecules are spliced to form single-stranded loops – a covalently closed structure [10]. Thus, this type of RNAs are relatively more stable in body fluid, such as blood plasma, urine and exosomes, providing an ideal easy-to-detect biomarker [11]. The RNA splicing, a critical process in genomic transcription, can manipulate genomic stability, transcriptome and chromatin organization, which may cause and promote cancer [12, 13]. For example, the alternative RNA splicing of androgen-receptor splice variant 7 messenger RNA (AR-V7) may cause the resistance of AR pathway inhibitors, leading to the progression of prostate cancer [14]. Backsplicing, which is very different from alternative splicing in linear RNAs, is a key process in circRNA biogenesis [15]. It has been hypothesized that the upstream site and downstream site of the circRNA carry the same repeat elements and the participating RBPs bring these two sites into proximity to constitute a loop structure [16, 17]. We have discovered that heterogeneous nuclear ribonucleoprotein L (HnRNP-L), a multi-functional RBP, is associated with pro-proliferation and anti-apoptosis activities in prostate tumor cells [18, 19]. Our study indicated that increase in the expression level of HnRNP-L in prostate cancer cells accelerates the disease progression, but the actual function of HnRNP-L in prostate cancer remains opaque. Because HnRNP-L is involved in the formation of circRNAs, this special RBP likely influences prostate tumor through the regulation of key circRNAs, promoting prostate cancer. For example, our analysis of four different publicly available datasets showed that circCSPP1 has higher expression in prostate cancer tissue than benign tissue, or higher expression in high-grade prostate cancer tissue than low-grade prostate cancer tissue;

while, an RNA immunoprecipitation (RIP) assay and mini-gene system data showed that circCSPP1 was modulated by HnRNP-L (see Results).

In the current study, we aim to establish the carcinomatous relevance of interactivity between HnRNP-L and circCSPP1 in prostate tumor. Bioinformatics analysis indicated that circCSPP1 can interfere with the complementary binding between miR-520 h and early growth response factor 1 (EGR1) – a well-known oncogene that causes tumorigenesis and metastasis in prostate cancer through the regulation of cell autophagy [20]. Therefore, we hypothesized that HnRNP-L regulates circCSPP1-miR-520 h-EGR1 axis to promote autophagy in prostate cancer cells, leading to tumor proliferation and metastasis. As indicated in Fig. 1, the increased expression of HnRNP-L likely upregulates the expression level of circCSPP1, which may sponge off miR-520 h in the cells and thereafter unleash ERG1. As a result, the highly expressed EGR1 protein will increase the transcription levels of autophagy related genes, promoting tumor proliferation and metastasis. In the study, we carried out various experiments to test these hypotheses, including western blot, confocal microscopy and transmission electron microscopy for gauging autophagy flux, loss of function and gain of function assays *in vitro* and *in vivo*, RIP and mini-genes system, and a series of bioinformatics analyses. Our data provided insights into circRNA-involved regulatory network that induces autophagy in prostate cancer cells which promote tumor progression.

Materials And Methods

Ethic statement

This study was approved by Ethics Committee of Zhujiang Hospital, Southern Medical University. The informed consents were signed by all the patients. According to the ethical and legal standards, every specimen was made and handled anonymously. All animal experiments in this study were carried out following the guidelines of the Institute for Laboratory Animal Research at Southern Medical University, Guangzhou, P. R. China.

Patient samples

Prostate cancer tissues and benign prostate hyperplasia tissues were respectively collected from 10 patients of Cancer Center of Guangzhou Medical University (Guangzhou, China) between 2018 and 2020. All the clinical and pathological information were summarized in Supplementary Table 2 and Table 3. Fresh tissues were viewed and approved by two pathologists, frozen immediately in liquid nitrogen, and stored at − 80 °C.

Cell culture

All the human prostate cancer cell lines including PC3, DU145, LNCaP and benign prostate hyperplasia cell line BPH-1, and human embryonic kidney cells (293T) were obtained from the Cell Bank of the Chinese Academy of Sciences (Shanghai, China). According to the instructions, PC3 was cultured in F12K medium (Procell), DU145 was cultivated in DMEM medium (Gibco), while 293T, LNCaP and BPH-1 were

maintained in RPMI-1640 medium (Gibco). All media listed above were supplemented with 10% fetal bovine serum (FBS, Gibco) and 1% Penicillin-Streptomycin (Gibco). All cell lines were maintained at 37 °C with 5% CO_2. For the autophagy induction experiments, all stable or transient transfected cell lines were maintained in Earle's balanced salt solution (EBSS) in the presence of 10μM Bafilomycin A1 (BAF) and/or 50nM Chloroquine (CQ) for 8 h. Dimethyl sulfoxide (DMSO) was used as negative control.

Transfection

The has_miR-520h mimics, pcDNA3.1-EGR1 and small interfering RNAs (siRNAs) targeting circCSPP1 or HnRNP-L were synthesized and transfected into cell lines using siRNA-Mate or GP-transfect-Mate (Genepharm) following the manufacturer's instruction. Lentivirus vectors encoding HnRNP-L, sh-/circCSPP1, sensGFP-stubRFP-LC3 and AGO2 were constructed and transfected into prostate cancer cell lines with Hitrans-GP (GeneChem). All the lentiviral transfected cells were treated with 1 μg/mL puromycin for 7 days to generate the stable cell lines. siRNA and miR-520 mimics sequence details are shown in Supplementary Table 1.

RNA extraction and real-time PCR

Total RNA was isolated from cells by using TRizol reagent (Takara, Tokyo, Japan) according to the instructions of manufacturer. Nuclear and cytoplasmic RNA fractions were separated from 10^2-10^7 cell pellets with the PARIS™ Kit (Ambion, Lifetechnologies) according to the manufacturer's instructions. RNA sample was treated with RNase R (Geneseed) at 37°C for 30 min to obtain purified circRNA. For circRNA and mRNA, cDNA was reverse-transcribed by using HiScript II Q RT SuperMix for qPCR (R223-01, Vazyme). For miRNA, cDNA was synthesized by using PrimeScript™ RT reagent Kit with gDNA Eraser (RR0471, Takara) with Bulge-Loop™ miRNA RT Primer (R10031.7, RIBOBIO). RT-qPCR was carried out using the SYBR Green Realtime PCR Master Mix (QPK-201, TOYOBO) with the CFX connect qPCR Detection System (Bio-Rad). β-actin was used as the endogenous control for mRNA and circRNA while U6 for microRNAs to calculate the relative fold changes for transcript abundance. Primers sequence details are shown in Supplementary Table 1.

Nucleic acid electrophoresis

The cDNA was augmented by RT-qPCR and gDNA was amplified using 2×Taq PCR MasterMix by T100™ Thermal Cycler (Bio-Rad). Then all type of PCR products were separated by 2% agarose gel electrophoresis with TAE running buffer. The electrophoresis was running at 110V for 40 min. Finally, the gels were irradiated by Ultraviolet rays and the targeted gene bands were measured by comparing with the DNA marker DL2000 (3427A, Takara).

Western blot analysis

For detecting relative autophagy markers LC3 and P62, cancer cells were treated with EBSS containing 10μM Bafilomycin A1 (BAF) or 50nM Chloroquine (CQ) for 8 h before lysed by RIPA buffer with PMSF on

ice for 15min. Then the cell lysis was mixed with 5× protein loading buffer and was subsequently denaturalized at 100℃ for 10 minutes. Total protein denaturants were separated by SDS-PAGE, transferred onto PVDF membranes (Millipore) and blocked with 5% skim milk in TBST for 1h. The membranes were incubated with primary antibodies against β-actin (BA2305, Boster), LC3A (NB100-2331, Novus), SQSTM1/P62 (sc-28359, Santa Gruz), HnRNP-L (ab6106, abcam), EGR1 (#4154 CST) at 4℃ overnight. Then, all the membranes were immersed in horseradish peroxidase-linked secondary antibodies against rabbit or mouse IgG. The bands were visualized using chemiluminescence imaging system (CLiNX ChemiScope Touch, Shanghai) and quantified by imageJ software.

RNA Immunoprecipitation assay

2×10^7DU145 cells were collected and lysed by ice-cold polysome lysis buffer with protease inhibitor and RNase inhibitor from the RNA Immunoprecipitation Kit (Bes5101, BersinBio). Major part (90%) of the cell lysis were incubated with anti-HnRNPL or AGO2 (IP group) and non-specific IgG (IgG group) respectively on vertical mixer at 4℃ for 16h, while the other was kept as an input group. Subsequently, two groups were mixed with protein A/G beads by vortex at 4℃ for 1h, followed by recovery of beads and RNA elution from the mixture. The RNA samples were quantified, reversely transcribed to cDNA and RT-qPCR analysis among IP, IgG and Input group.

Fluorescence in situ hybridization (FISH)

1×10^4cells were embedded to cover slide in a 48-well plate and cultured overnight. PCa cells were fixed by 4% paraformaldehyde for 15 min at room temperature after washed with 1X phosphate-buffered saline (PBS) for 5 min x 2 and then penetrated with 0.1% Triton X-100. Subsequently, cells were washed with 1X PBS for 5 min x 2 and treated with 2× SSC for 30 min at 37 °C. The probes (PA20190412001, RiboBio) targeting circCSPP1/EGR1/has_miR-520h were pre-mixed with hybridization buffer and denatured at 73 °C for 5 min. After hybridization, the slides were washed with 0.1% Tween 20 for 5 min at 42°C, and then washed with 2 × SSC at 42°C for 5 min × 2. DAPI was re-dyed at dark room temperature for 20 min and washed with 1X PBS, 5 min x 2. Treatment of antifade reagent and the cell slides were adhered to the slide (face up) with neutral gum before the observation under fluorescence microscope.

Luciferase Reporter Assay

Dual luciferase reporter vector pmirGLO (Promega) was used for the luciferase assays. circCSPP1/EGR-1 wild-type (circCSPP1/EGR-1 WT) and mutant (circCSPP1/EGR-1 MUT) reporter vectors were constructed and inserted into the pmirGLO. 5×10^5cells were seeded into a 12-well plate and cultured for 24h at 37℃ with 5% CO_2. Subsequently, 1.6μg reporter plasmids (circCSPP1/EGR-1 WT, circCSPP1/EGR1 MUT) together with 20μM has_miR-520h mimics or negative control were transfected into DU145/PC3 cells. Then the transfected cells were transferred to the incubator and cultured for another 48h. Finally, the Dual-Luciferase Reporter System Kit (Promega) was used to detect the luciferase activity with Tecan M1000 microplate reader.

Electron microscopy

Adherent cells estimated at 1 ×10^6 were treated with 0.25% trypsin for only 30 seconds to keep cell membrane intact. Cell suspension was centrifuged at 800 rpm for 5min following by supernatant removal. Each sample was fixed with 2% glutaraldehyde at 4℃ for over 15 min and washed with PBS three times for 10min each. Samples were post-fixed with 1% OsO4 followed by an ascending gradient dehydration step of ethanol and infiltration with propylene oxide. After ultrathin sectioning and staining with 3% lead citrate- uranyl acetate, samples were observed under an electron microscope (HT-7800, Hitachi High-tech).

Examination of autophagy flux

PC3 and DU145 cells were cultured and transfected with lentivirus carrying sensGFP-stubRFP-LC3 at 37 °C for 48 h. Next, the transfected cells were treated with EBSS containing 50μM BAF for 8 h. Cells were fixed with 4% paraformaldehyde for 30 min. Finally, the autophagy flux was analyzed using a confocal fluorescence microscopy (Leica, Germany). In merged images, yellow spots represent autophagosomes while red spots represent autolysosomes.

Cell proliferation and Colony formation assays

Cell proliferation was determined using CCK-8 assays (MA0218-5, Meilunbio). The transfected cells were seeded into 96-well plates at a density of 3000 cells per well. 100μl complete medium containing 10μl CCK-8 reagent was added into each well at 0, 24, 48, 72, 96h after seeding. All plates were scanned using a microplate reader (Bio-Rad) in another 2h incubation. The absorbance at 450nm was measured and analyzed. PCa cells were plated at an initial density of 500 cells per well in a 6-wells plate and cultured at 37°C with 5% CO_2 for 14 days. Then, the colonies were fixed for 20 min with 4% paraformaldehyde and stained for 15 min with crystal violet. After discarding the staining solution, the plates were air-dried at room temperature and then observed under the light microscope.

Migration and invasion assay

Wound healing assays were carried out to evaluate the migration ability of PCa cells. Transfected cells were seeded in 6-well plates at a density of 1 ×10^6 cells/well and grown to 90-100% in 10% FBS medium. Then linear wounds were scratched with a sterile 200μL plastic pipette tip in each well and PBS was used to remove the detached cells. Cells were cultured in FBS free medium to inhibit cell proliferation. Images of the scratched area was captured at indicated times (0 and 24h) using a Leica light microscope. For invasion assay, the transwell chamber was precoated with Matrigel (), and 6×10^4 cells were seeded to the upper chamber. Subsequently, 500 μL of DMEM medium containing 10% FBS was added to the lower chamber. The cells on the top surface were removed with a cotton ball after incubation for 24 h, and the cells that invaded to the lower membrane surface were fixed with 4% paraformaldehyde and stained with 0.1% crystal violet solution. The invaded cells were then photographed and counted under an inverted microscope.

Animal experiments

The 4-week old C57BL/6 nude mice (male) were obtained from Guangdong Experimental Animal center (Guangzhou, China). 6 male C57BL/6 mice were subcutaneously injected with 3 × 10^6 stably-transfected DU145 cells (empty vector or circCSPP1-overexpression) in both back sides. The growth of implanted PCa tumors was monitored by measuring their volumes every 3 days. Finally, the mice were sacrificed and their xenografts were measured and photographed.

Statistical analysis

All data were shown as mean ± SD processed by GraphPad Prism 7.0 (La Jolla, USA). Student's t-test analysis was used to evaluate the normalized data. Pearson correlation assay was used to analyze expression correlation (circCSPP1, miR-520h and EGR1). Kaplan-Meier method was used to estimate the Overall survival (OS) and Biochemical recurrence (BCR) curve. All statistical tests were two-sided and considered statistically significant when p values are less than 0.05.

Results

CircCSPP1 is upregulated in prostate cancer

Four publicly available datasets, including two microarrays [21, 22], GSE21036 and TCGA_PARD, were analyzed, which indicated that circCSPP1 was always associated with prostate cancer and its progression (Fig. 2A). The results showed that the expression level of circCSPP1 was higher in prostate cancer tissues than that in benign tissues, and it was also upregulated in high-grade prostate cancer tissues compared to the low-grade prostate cancer tissues (Figure S1A-1B). The survival analysis indicated that the mRNA expression level of CSPP1, the parent gene of circCSPP1, was positively associated with the overall survival (OS) and biochemical recurrence (BCR) free survival in prostate cancer, i.e., patients with higher CSPP1 expression had significantly worse outcomes than those with lower CSPP1 expression (Figure S1C-1D). We found that circCSPP1, the annotation of which is shown in the Circular RNA Interactome (Figure S1E), is derived from exons 8–11 and the back-splicing site was identified by Sanger sequencing (Fig. 2B). To further verify the differential expression of circCSPP1 in prostate cancer cells (C4-2, LNCaP, 22Rv1, DU145, PC3) or benign cells (BPH-1) as well as prostatic tissues, we designed qPCR primers and fluorescent probes specifically targeting the back-splicing site of circCSPP1. The results of qPCR showed that the expression of circCSPP1 was significantly higher in prostate cancer cells (LNCaP, 22Rv1, DU145 and PC3) than in benign cells (BPH-1), and it was also higher in prostate cancer tissues than in non-cancerous tissues (Fig. 2C,2D & Figure S1E-G). The experiment of RNase R treatment showed that circCSPP1 was resistant to the RNase R digestion activity and remained stable (Fig. 2E). When compared with genomic DNA (gDNA) group, circCSPP1 could be amplified by divergent primers in cDNA sample, and their PCR products were validated by agarose gel electrophoresis (Fig. 2F). Furthermore, the subcellular fractionation and Fluorescence in situ hybridization (FISH) analysis showed that circCSPP1 was mainly localized in the cytoplasm in DU145 and PC3 (Fig. 2I&2J).

CircCSPP1 promotes prostate cancer in vitro and in vivo

Two small interference RNAs, si-circCSPP1-1 and si-circCSPP1-2, were designed to target the back-splicing junction of circCSPP1, both of which had significantly reduced the expression of circCSPP1 but not the linear form of CSPP1 (linear-CSPP1) in DU145 and PC3 (Figure S2C). We then constructed stable cell lines, including DU145 and PC3, with transfection of lentivirus-circCSPP1 or circCSPP1-sh1/2. RT-qPCR results showed that these lentivirus vectors can increase/decrease the expression level of circCSPP1 in DU145 and PC3 cells, without affecting the mRNA or protein expression of CSPP1 (Fig. 3A, S2G, S2H&S2I). The wound healing and transwell assays indicated that overexpression of circCSPP1 promoted migration and invasion of DU145 and PC3 compared with the controls, and *vice versa* (Fig. 3B&3C). The CCK-8 and plate colony formation assays revealed that circCSPP1 overexpression accelerated the proliferation of DU145 and PC3, and *vice versa* (Fig. 3D&3E). We then injected DU145 cells with lentivirus-circCSPP1 or control subcutaneously on both sides of 6 nude mice, and the result of *in vivo* experiments showed that tumors with implantation of circCSPP1 overexpression grew faster and bigger than the control group (Fig. 3F).

CircCSPP1 promotes prostate cancer autophagy in vitro

To find out in what mechanism cricCSPP1 potentially regulated the progression of PCa cell lines, we carried out the Next Generation Sequencing of DU145 with the overexpression of circCSPP1 (Figure S2A). The KEGG pathway analysis with differentially expressed genes ($P < 0.01$, $\log^2FC \geq 1.5$ or $\log^2FC \leq -1.5$) showed that circCSPP1 might facilitate PCa progression via regulating autophagy (Figure S2B). Thus, to test what kind of role circCSPP1 plays in autophagy process, DU145 and PC3 were both treated in starvation condition with Earle's Balanced Salt Solution (EBSS) at a time gradient of 0 h, 2 h, 4 h, and 6 h, and the results from the RT-qPCR experiments showed that the expression level of circCSPP1 increased over time gradient (Figure S2D). Then western blotting was conducted and the results showed that while knocking down circCSPP1 by siRNA, the conversion levels of LC3-II and P62, two autophagy-related markers, did not change in DU145 and PC3 if these cells were maintained in complete medium for 8 hours with or without BAF treatment (Figure S2E). When cultured in EBSS, however, the conversion of LC3-II and P62 of these prostate cancer cell lines treated with the BAF increased significantly compared with the cell lines in DMSO condition (Figure S2E). In addition, to examine whether blocking autophagy could influence circCSPP1 expression, DU145 and PC3 were treated with BAF at a concentration gradient of 0 μM, 5 μM, and 10 μM, respectively. The RT-qPCR assays showed that blocking autophagy exerted no effect on circCSPP1 expression (Figure S2F), indicating that circCSPP1 may act as an upstream regulator in autophagy modulation. Then we also tested this hypothesis in stable cell lines. Western blotting showed that circCSPP1-sh1/2 also displayed an autophagic inhibition effect, whereas circCSPP1 overexpression remarkably increased the conversion of LC3-II and P62 in DU145 and PC3 cells treated in EBSS (Fig. 4A&B). Meanwhile, the confocal fluorescence microscopy showed that overexpression/knock-down of circCSPP1 obviously increased/reduced the accumulation of autophagolysosomes in DU145 and PC3 cells (Fig. 4C). These results were consistent with the variation of the numbers of autophagosomes exhibited in DU145 and PC3 cells with the overexpression or knock-down of circCSPP1

through transmission electron microscopy (Fig. 4D). Furthermore, to exclude the influence of linear-CSPP1 on autophagy, we designed 3 siRNAs targeting different sites of CSPP1, which significantly knocked down mRNA and protein levels of CSPP1 in RT-qPCR and western blot experiments, respectively (Figure S2G&2H), but did not affect the expression level of circCSPP1. Notably, knockdown of CSPP1 had no effect on autophagy in DU145 and PC3 (Figure S2H).

Interaction between circCSPP1 and miR-520 h

Since circCSPP1 was primarily situated in the cytoplasm, we assumed that it is likely involved in competing endogenous RNA (ceRNA) network to regulate miRNAs that may be critical to progression of prostate cancer cells. Bioinformatics analyses, including the prediction of target miRNAs for circCSPP1 (circularRNA Interactome) and the detection of autophagy associated miRNAs (GeneCards and microRNA.org), identified 5 common miRNAs, i.e., miR-197-3p, miR-324-5p, miR-375-3p, miR-431-5p and miR-520 h (Fig. 5A). The analysis of TCGA and GEO datasets (TCGA_PARD, GSE8126, GSE21036) showed that miR-197-3p, miR-324-5p and miR-375-3p were upregulated in prostate cancer tissues than in tumor-adjacent pathologically normal tissues (Fig. 5B). A RT-qPCR analysis was performed to further test the expression of miR-431-5p and miR-520 h in prostate cancer cells, which showed that they were both downregulated (Fig. 5C). Nevertheless, the *in vitro* analyses of overexpression/knock-down of circCSPP1 showed that only miR-520 h was reduced/elevated accordingly (Fig. 5D). In addition, the RIP experiment with AGO2 antibody followed by the RT-qPCR assays and agarose gel electrophoresis confirmed that circCSPP1 was enriched in AGO2-IP analysis, suggesting an AGO2-involved complementary binding between circCSPP1 and target miRNAs (Fig. 5E). Then the FISH analysis was employed to study circCSPP1 and miR-520 h, which showed that they were co-localized in the cytoplasm (Fig. 5F). Based on the predicted binding sites of miR-520 h in the circCSPP1 sequence, dual-luciferase reporter vectors of wild-type (WT) sequences and the mutant (MUT) sequence of circCSPP1 are constructed. The results showed that the luciferase activity of WT reporters was significantly reduced by miR-520 h mimics compared with controls (Fig. 5G).

CircCSPP1 sponges off miR-520 h to promote tumor migration, invasion, proliferation and autophagy in vitro

To further understand the role of miR-520 h and circCSPP1 in promoting prostate cancer progression, we performed rescue experiments, including wound healing, transwell, CCK-8 and plate colony formation assays to investigate the effects of circCSPP1/miR-520 h axis in DU145 and PC3 cells. Wound healing and transwell assays showed that circCSPP1 promoted DU145 and PC3 cells migration and invasion, while the miR-520 h mimics attenuated this promotion (Fig. 6A&6B). The colony formation assay and CCK-8 assays demonstrated that circCSPP1 increased the proliferation ability of DU145 and PC3 cells, while the miR-520 h mimics weakened such an association (Fig. 6C&6D). We also conducted a series of rescue experiments to confirm the essential role of miR-520 h in the autophagy activity of prostate cancer cells. The western blotting indicated that the conversion of LC3-II and the degradation of P62 protein induced by circCSPP1 were abrogated by the miR-520 h mimics (Fig. 6F). Furthermore, autophagy flux

monitoring with sensGFP-stubRFP-LC3 and autophagosomes observation by TEM showed that the number of LC3-II puncta (yellow) and autophagosomes elevated by circCSPP1 were significantly suppressed by the miR-520 h mimics (Fig. 6F&6G).

EGR1 regulated by circCSPP1/miR-520 h axis

We explored whether circCSPP1/miR-520 h axis regulates the expression of autophagy-related genes by targeting their 3'UTR. We performed RNAseq analysis for DU145 cells with lentivirus-NC and lenticirus-circCSPP1, respectively, each with three replicates. The differentially expressed genes are shown in Figure S2A. The bioinformatics algorithms and publicly available datasets, including StarBase, miRWalks, and GeneCards, were used to identify the miR-520 h-target genes from the differentially expressed genes detected in our RNAseq data, yielding EGR1 – an important oncogene for many cancers (Fig. 7A). Then we examined the expression of EGR1 in prostate cancer cell lines with the transfection of miR-520 h mimics. As shown in Fig. 7B&7C, both the mRNA and protein expression level of EGR1 were suppressed by miR-520 h mimics compared to the controls. The FISH was conducted which showed that EGR1 and miR-520 h were co-localized in the cytoplasm in PC3 cells (Fig. 7D). The EGR1 luciferase activity of WT reporters were significantly reduced by miR-520 h mimics compared to the controls and the mutation group (Fig. 7E). We also employed RT-qPCR to verify the expression of circCSPP1, miR-52 h and EGR1 in prostate cancer tissues and benign tissues. The results showed that the expression levels of circCSPP1 and EGR1 were higher in the prostate cancer tissues than those in the benign tissues, whereas, the expression of miR-520 h was lower in the prostate cancer tissues than that in the benign tissues (Fig. 7F). The expression level of circCSPP1 was positively correlated with that of EGR1, whereas miR-520 h exhibited a negative correlation with circCSPP1 or EGR1 mRNA. We observed the similar correlation patterns in xenograft tumor derived from DU145 cells with circCSPP1 overexpression (Fig. 7G).

Inhibition of migration, invasion, proliferation and autophagy in vitro **by the silenced EGR1 through miR-520 h**

Cell migration, invasion, proliferation abilities and autophagy activities were gauged in prostate cancer cells to investigate whether EGR1 was targeted and regulated by miR-520 h. The results revealed that overexpression of EGR1 significantly promoted the proliferation, migration and invasion in prostate cancer cells. However, introduction of miR-520 h mimic rescued these EGR1 related phenotypes in CCK-8, colony formation assays, wound healing and transwell assays (Fig. 8A & 8B). Additionally, the western blot showed that overexpression of EGR1 significantly increased the conversion of LC3-II and P62 and these effects were also rescued by the introduction of miR-520 h mimic. Moreover, the results of confocal fluorescent microscopy and TEM showed that miR-520 h mimic clearly attenuated the acceleration of autophagy flux and accumulation of autophagosomes induced by EGR1 (Fig. 8D & 8E).

CircCSPP1 is regulated by HnRNP-L

Enlighten by a recent study where HnRNP-L was reported to be responsible for a series of circular RNA biogenesis by alternative splicing in LNCaP, we hypothesized circCSPP1, regulated by HnRNP-L, plays a critical role to promote aggressive phenotypes in prostate cancer cells. The differential expression analysis of the dataset GSE72844 showed that circCSPP1 was significantly downregulated when HnRNP-L was knocked down (Fig. 9A). Then we constructed prostate cancer cell lines with HnRNP-L overexpression or knockdown through stable or transient transfection. By employing RT-qPCR and Western blot, HnRNP-L was significantly downregulated by si-HnRNP-L (Figure S3A&B) or overexpressed by lentivirus stably encoding HnRNP-L (Figure S3C&D). Further RT-qPCR analysis showed that knockdown or overexpression of HnRNP-L reduced circCSPP1 expression by 60–70% or upregulated circCSPP1 expression in 3–7 times compared to NC group. However, the abundance of linear-CSPP1 mRNA did not change while knocking down or overexpressing HnRNP-L. (Fig. 8B&C). Subsequently, we conducted a RIP assay followed by agarose gel electrophoresis, which unveiled that circCSPP1 bound to HnRNP-L (Fig. 9D). Nevertheless, the molecular mechanism how HnRNP-L regulates the biogenesis of circCSPP1 needs to be further elucidated. Therefore, we rearranged the FASTQ-type data of the RNAs captured by HnRNP-L or non-specific IgG in the RIP assays, provided in GSE72841 [18]. With an advanced analysis of RIP-sequencing data and the transcripts of the corresponding parent gene in the integrative genomic viewer (IGV), we found 5 potential CA-rich motifs of CSPP1 pre-mRNA, which may be the potential binding sites for HnRNP-L (Fig. 9E). These specific motifs contained CA repeats of a variety of lengths. To test the hypothesis that circCSPP1 is regulated by HnRNP-L, we designed 5 specific primers targeting these 5 motifs. The RIP using HnRNP-L antibody and RT-qPCR analysis showed that the motif sequences represented by primers 3 & 4 were successfully amplified (Fig. 9F & 9G). To further verify that these two motifs are the potential sites for HnRNP-L binding and also for alternative splicing, we constructed a mini-gene vector by interposing CA-repeat motifs to the flanking introns, on either or both sides, of GAPDH (Fig. 9H). To evaluate the efficiency in forming GAPDH circRNA catalyzed by HnRNP-L, the mini-gene constructs were transfected into HEK293T cells followed by RT-qPCR assays. The results showed that these CA-repeat motifs inserted to the flanking introns remarkably enhanced GAPDH circRNA formation, especially when the insertion occurred in both flanking sides (Fig. 9I). Meanwhile, a siRNA targeting HnRNP-L mRNA was designed for HnRNP-L significantly decreased the GAPDH circRNA abundance in HEK293T cells (Fig. 8J). In conclusion, these data demonstrated that the high level of circCSPP1 could be an outcome of upregulation by HnRNP-L involved alternative splicing.

Discussion

CircRNAs has drawn increasing attention from the research field of noncoding RNAs. Dysregulations in circRNAs have been reported in a variety of cancers, including melanoma [23], bladder cancer [24], hepatocellular carcinoma [25], and glioma [26]. Although circCSPP1 was recently reported to be associated with tumor proliferation, invasion and migration in ovarian cancer [27], and Colorectal Carcinoma [28], its circular structure has not been confirmed in these studies. In this study, we used a combination of RNase R test, divergent primers, convergent primers and sanger sequencing to definitively demonstrated the circularization of exon #8 to exon #11 of the parent gene CSPP1 which has two

primary isoforms: CSPP and CSPPL [29]. Previous study indicated that the inhibition of CSPP/CSPPL could induce G1 phase arrest in cell cycle and the destabilization of desmosomes [30, 31]. Nevertheless, how CSPP1 functions in prostate cancer remains unclear. The expression of linear CSPP1 did not change significantly in the circCSPP1 overexpressed/knockdown cell lines, indicating that we can focus on the function investigation on circCSPP1 without confounding with linear CSPP1. The study showed that the overexpression of circCSPP1 promoted autophagy which induced tumor progression, and this phenomenon became more apparent after the EBSS starvation, and *vice versa*. It was interesting to observe that overexpression of circCSPP1 promoted autophagy but not the linear CSPP1.

Mounting evidences have shown that noncoding RNAs, including lncRNAs and miRNAs, were involved in autophagy related tumor progression [32, 33]; however, circRNAs have been rarely reported to be related to either autophagy or cancer progression, especially for prostate cancer. The previous research indicated that circRNAs play critical roles in various cellular functions, including competing endogenous RNA (CeRNA), translating peptides, regulating transcription, scaffold for protein complexes and so on [10]. This study focused on deciphering the mechanistic relationship between circCSPP1, autophagy, and tumor progression in prostate cancer. According to our data, circCSPP1 was mainly localized in the cytoplasm and AGO2 RIP showed that circCSPP1 bound to AGO2, suggesting circCSPP1 acted as a miRNA sponge. Bioinformatics analysis was used to search for the candidate miRNAs that bind to circCSPP1, leading to the identification of miR-520 h as the downstream target of circCSPP1.

The analysis of publicly available datasets as well as our own patient samples indicated that miR-520 h inhibited autophagy and tumor proliferation, migration and invasion in prostate cancer. The FISH and dual-luciferase reporter assay showed that miR-520 h is a direct target of circCSPP1. The bioinformatics analysis of multiple relevant datasets, shown in the Venn diagram in Fig. 6B, indicated that EGR1 is the only common gene (or mRNA). We confirmed that EGR1 was a direct target of miR-520 h by the qPCR, FISH and dual-luciferase reporter assay. The rescue experiment using miR-520 h mimics indicated that EGR1 can promote cell vitality, migration, invasion by inducing autophagy and such effect may be countered by miR-520 h partly. Finally, we verified the association among circCSPP1/miR-520 h/EGR1 axis in our prostate cancer samples and as well as using the experiment with xenografts. It has been reported that EGR1 regulated autophagy by transcriptionally affecting autophagy-associated gene expression, including LC3B [20]. Further investigation is warranted to identify other importance autophagy-associated gene regulated by EGR1 in prostate cancer.

The circRNAs form by the back-splicing of pre-mRNA – a new type of alternative splicing [10]; however, the complete process of the biogenesis of circRNAs is yet clear. Interestingly, circCSPP1 was remarkably downregulated by si-HnRNP-L (GSE72844) [18], suggesting that HnRNP-L is a critical factor in this alternative splicing and regulates circRNA formation. In the study, the data of the RIP with HnRNP-L antibody suggested that the pre-RNA of circCSPP1 contains two out of five CA-rich regions which are likely the binding sites for HnRNP-L. We further verified these two CA-rich binding sites in the flanking introns upregulated circCSPP1 by the mini-gene system. Nevertheless, these experiments were performed

in vitro; other studies, such as the CRISPR/Cas9 mouse experiments or fluorescence resonance energy transfer (FRET) assay, are needed for further validation.

Conclusion

In summary, our study illustrated the association between HnRNP-L, circCSPP1, miR-520 h and EGR1 in prostate cancer and the potential underlying mechanism to promote prostate cancer. Overexpression of HnRNP-L upregulates circCSPP1 and influences circCSPP1/miR-520 h/EGR1 axis, which then induces autophagy and eventually promotes prostate cancer to grow, migrate and invade. The data and results provide new insights to understanding the role of circRNAs in regulating autophagy in prostate cancer.

Abbreviations

PCa: Prostate cancer; CSPP1:centrosome and spindle pole associated protein 1; HnRNP-L:heterogeneous nuclear ribonucleoprotein L; TME:Transmission electron microscope; ceRNA:competing endogenous RNA; AGO2:argonaute RISC catalytic component 2; RT-qPCR:quantitative real-time polymerase chain reaction; EGR-1:early growth response factor 1.

Declarations

Acknowledgements

Not applicable.

Authors' Contributions

Xiangming Mao and Jianming Lu conceived of the study and Chuanfan Zhong carried out its design. Jianming Lu, Chuanfan Zhong and Fangpeng Shu performed the experiments. Daojun Lv, Xiao Tan, Shuo Wang, Kaihui Wu, Taowei Yang and Weibo Zhong collected clinical samples. Jianming Lu, Daojun Lv, Yuehan Li, Bin Wang and Yanfei Chen analyzed the data. Yaguang Zou provided administrative or technical support. Jianming Lu, Chuanfan Zhong, Weide Zhong and Zhenyu Jia wrote the paper. All authors participated in writing the manuscript and approved the final version.

Funding

This research was supported by grants from National Natural Science Foundation of China (81773277, 82003271, 82072813); China postdoctoral science foundation (2019M662979, 2018M643126 and 2019M662865); Science and Technology Program of Guangzhou (201803010014). Guangdong Basic and Applied Basic Research Foundation (No.2019A1515110033). Guangzhou Municipal Science and Technology Project (201803040001). Guangdong Medical Science Research Project (A2020544).

Availability of data and materials

The RNA-seq data of stable PCa cell lines (DU145-vector; DU145-circCSPP1, GSE158975) analyzed during this study are included in this published article and its supplementary information files.

Ethics approval and consent to participate

The present study was approved by the Ethics Committee of Zhujiang Hospital, Southern Medical University.

Consent for publication

Not applicable.

Competing interests

The authors declare that they have no competing interests.

References

1. Siegel RL, et al. Cancer statistics, 2020. CA: a cancer journal for clinicians. 2020; 70(1): 7-30.
2. Bray F, et al. Global cancer statistics 2018: GLOBOCAN estimates of incidence and mortality worldwide for 36 cancers in 185 countries. CA Cancer J Clin. 2018; 68(6): 394-424.
3. Cheng HH, et al. Germline and Somatic Mutations in Prostate Cancer for the Clinician. J Natl Compr Canc Netw. 2019; 17(5): 515-21.
4. Dong X, Chen R. Understanding aberrant RNA splicing to facilitate cancer diagnosis and therapy. Oncogene. 2020; 39(11): 2231-42.
5. Santanam U, et al. Atg7 cooperates with Pten loss to drive prostate cancer tumor growth. Genes Dev. 2016; 30(4): 399-407.
6. Howard N, et al. New developments in mechanisms of prostate cancer progression. Semin Cancer Biol. 2019; 57(111-16.
7. Anastasiadou E, et al. Non-coding RNA networks in cancer. Nat Rev Cancer. 2018; 18(1): 5-18.
8. Hua JT, et al. Landscape of Noncoding RNA in Prostate Cancer. Trends Genet. 2019; 35(11): 840-51.
9. Liu J, et al. Circular RNAs: The star molecules in cancer. Mol Aspects Med. 2019; 70(141-52.
10. Kristensen LS, et al. The biogenesis, biology and characterization of circular RNAs. Nat Rev Genet. 2019; 20(11): 675-91.
11. Chen B, Huang S. Circular RNA: An emerging non-coding RNA as a regulator and biomarker in cancer. Cancer Lett. 2018; 418(41-50.
12. Sveen A, et al. Aberrant RNA splicing in cancer; expression changes and driver mutations of splicing factor genes. Oncogene. 2016; 35(19): 2413-27.
13. Robinson TJ, et al. Alternative RNA Splicing as a Potential Major Source of Untapped Molecular Targets in Precision Oncology and Cancer Disparities. Clin Cancer Res. 2019; 25(10): 2963-68.

14. Cai L, et al. ZFX Mediates Non-canonical Oncogenic Functions of the Androgen Receptor Splice Variant 7 in Castrate-Resistant Prostate Cancer. Mol Cell. 2018; 72(2): 341-54.
15. Kristensen LS, et al. The biogenesis, biology and characterization of circular RNAs. Nat Rev Genet. 2019; 20(11): 675-91.
16. Errichelli L, et al. FUS affects circular RNA expression in murine embryonic stem cell-derived motor neurons. Nat Commun. 2017; 8(14741.
17. Conn SJ, et al. The RNA binding protein quaking regulates formation of circRNAs. Cell. 2015; 160(6): 1125-34.
18. Fei T, et al. Genome-wide CRISPR screen identifies HNRNPL as a prostate cancer dependency regulating RNA splicing. Proc Natl Acad Sci U S A. 2017; 114(26): E5207-15.
19. Zhou X, et al. HnRNP-L promotes prostate cancer progression by enhancing cell cycling and inhibiting apoptosis. Oncotarget. 2017; 8(12): 19342-53.
20. Peeters J, et al. Transcriptional and epigenetic profiling of nutrient-deprived cells to identify novel regulators of autophagy. Autophagy. 2019; 15(1): 98-112.
21. Yang Z, et al. Dysregulation of p53-RBM25-mediated circAMOTL1L biogenesis contributes to prostate cancer progression through the circAMOTL1L-miR-193a-5p-Pcdha pathway. Oncogene. 2019; 38(14): 2516-32.
22. Jin C, et al. Silencing circular RNA circZNF609 restrains growth, migration and invasion by up-regulating microRNA-186-5p in prostate cancer. Artif Cells Nanomed Biotechnol. 2019; 47(1): 3350-58.
23. Hanniford D, et al. Epigenetic Silencing of CDR1as Drives IGF2BP3-Mediated Melanoma Invasion and Metastasis. Cancer Cell. 2020; 37(1): 55-70.
24. Chen X, et al. PRMT5 Circular RNA Promotes Metastasis of Urothelial Carcinoma of the Bladder through Sponging miR-30c to Induce Epithelial-Mesenchymal Transition. Clin Cancer Res. 2018; 24(24): 6319-30.
25. Yu J, et al. Circular RNA cSMARCA5 inhibits growth and metastasis in hepatocellular carcinoma. J Hepatol. 2018; 68(6): 1214-27.
26. Chen J, et al. circPTN sponges miR-145-5p/miR-330-5p to promote proliferation and stemness in glioma. J Exp Clin Cancer Res. 2019; 38(1): 398.
27. Li QH, et al. circ-CSPP1 promotes proliferation, invasion and migration of ovarian cancer cells by acting as a miR-1236-3p sponge. Biomed Pharmacother. 2019; 114(108832.
28. Wang Q, et al. CircCSPP1 Functions as a ceRNA to Promote Colorectal Carcinoma Cell EMT and Liver Metastasis by Upregulating COL1A1. Front Oncol. 2020; 10(850.
29. Shearer RF, et al. The E3 ubiquitin ligase UBR5 regulates centriolar satellite stability and primary cilia. Mol Biol Cell. 2018; 29(13): 1542-54.
30. Hauge H, et al. Characterization of the FAM110 gene family. Genomics. 2007; 90(1): 14-27.

31. Sternemalm J, et al. CSPP-L Associates with the Desmosome of Polarized Epithelial Cells and Is Required for Normal Spheroid Formation. Plos One. 2015; 10(8): e134789.
32. Wang S, et al. MicroRNA-125b Interacts with Foxp3 to Induce Autophagy in Thyroid Cancer. Mol Ther. 2018; 26(9): 2295-303.
33. Li P, et al. ZNNT1 long noncoding RNA induces autophagy to inhibit tumorigenesis of uveal melanoma by regulating key autophagy gene expression. Autophagy. 2020; 16(7): 1186-99.

Figures

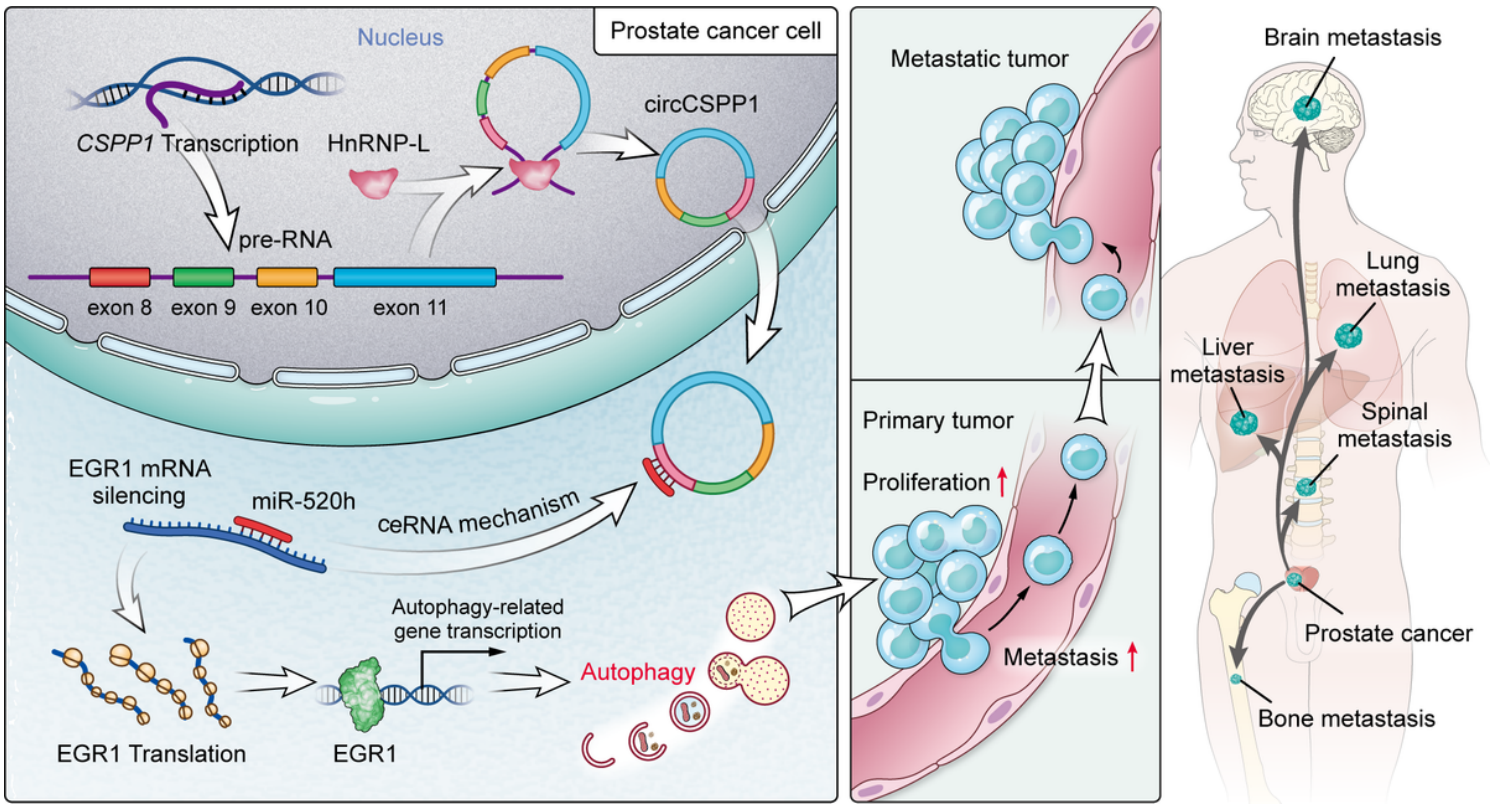

Figure 1

A schematic model presenting that circCSPP1 is up-regulated by HnRNP-L and circCSPP1/miR-520h/EGR-1 axis promotes prostate cancer progression through autophagy.

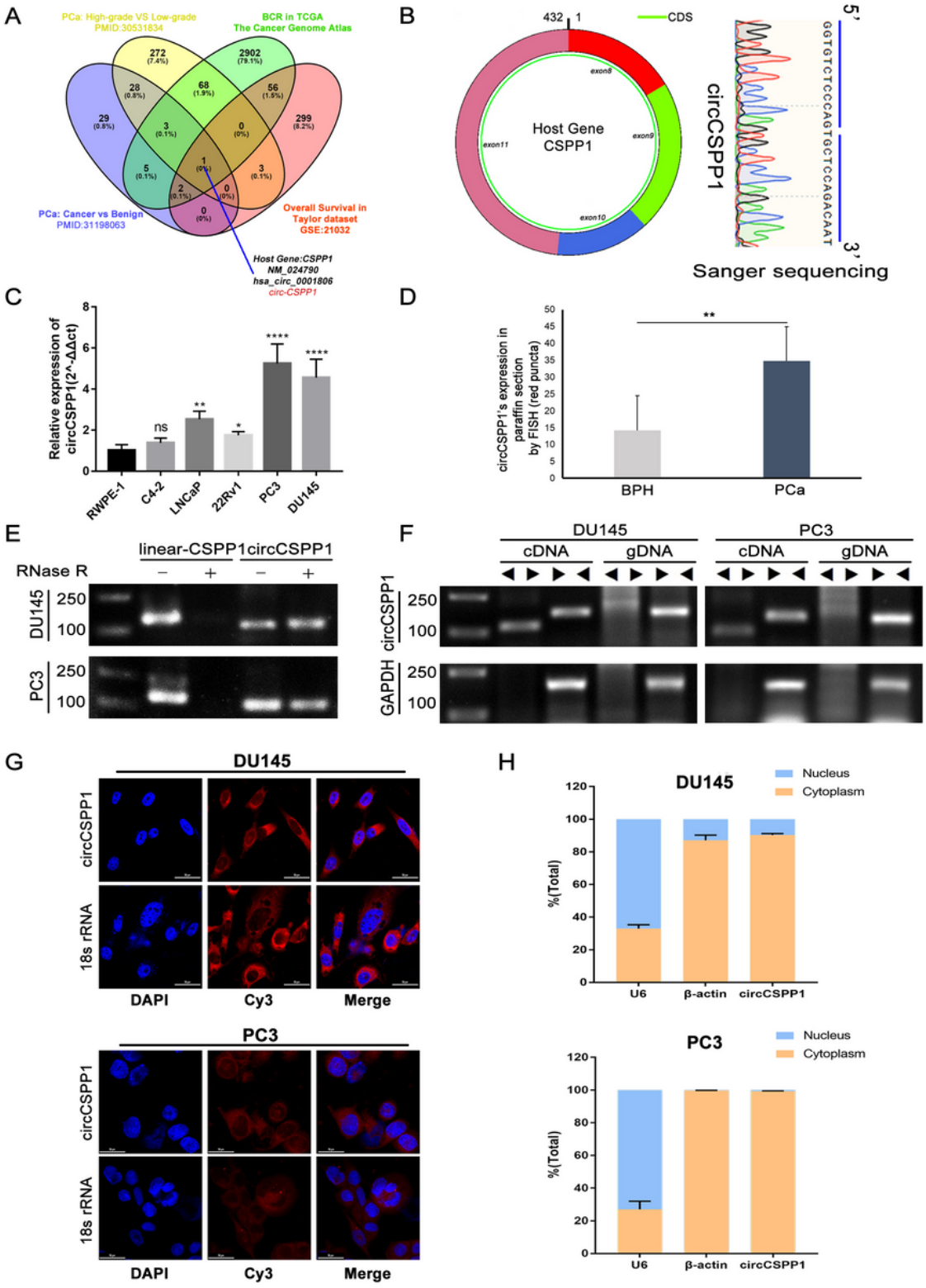

Figure 2

Analysis of circCSPP1 expression in human PCa tissues and cell lines. (A) Venny diagram shows circCSPP1 is the only gene in the overlap. (B) Sanger sequencing detected the back-splicing site of circCSPP1. (C) Naive expression of circCSPP1 in prostatic cell lines, Student's t test, ****P<0.0001, ***P<0.001. (D) Expression of circCSPP1 in clinical samples, **P<0.01. (E) RNase R resistance test of circCSPP1. (F) Divergent and convergent primers were used to detect circCSPP1 via RT-qPCR in PCa cell

lines. (G) FISH of circCSPP1 (red) combined with nuclear DAPI staining (blue) in PCa cell lines. (H) Subcellular distribution of circCSPP1 was detected by Nuclear and cytoplasmic separation assay in PCa cell lines.

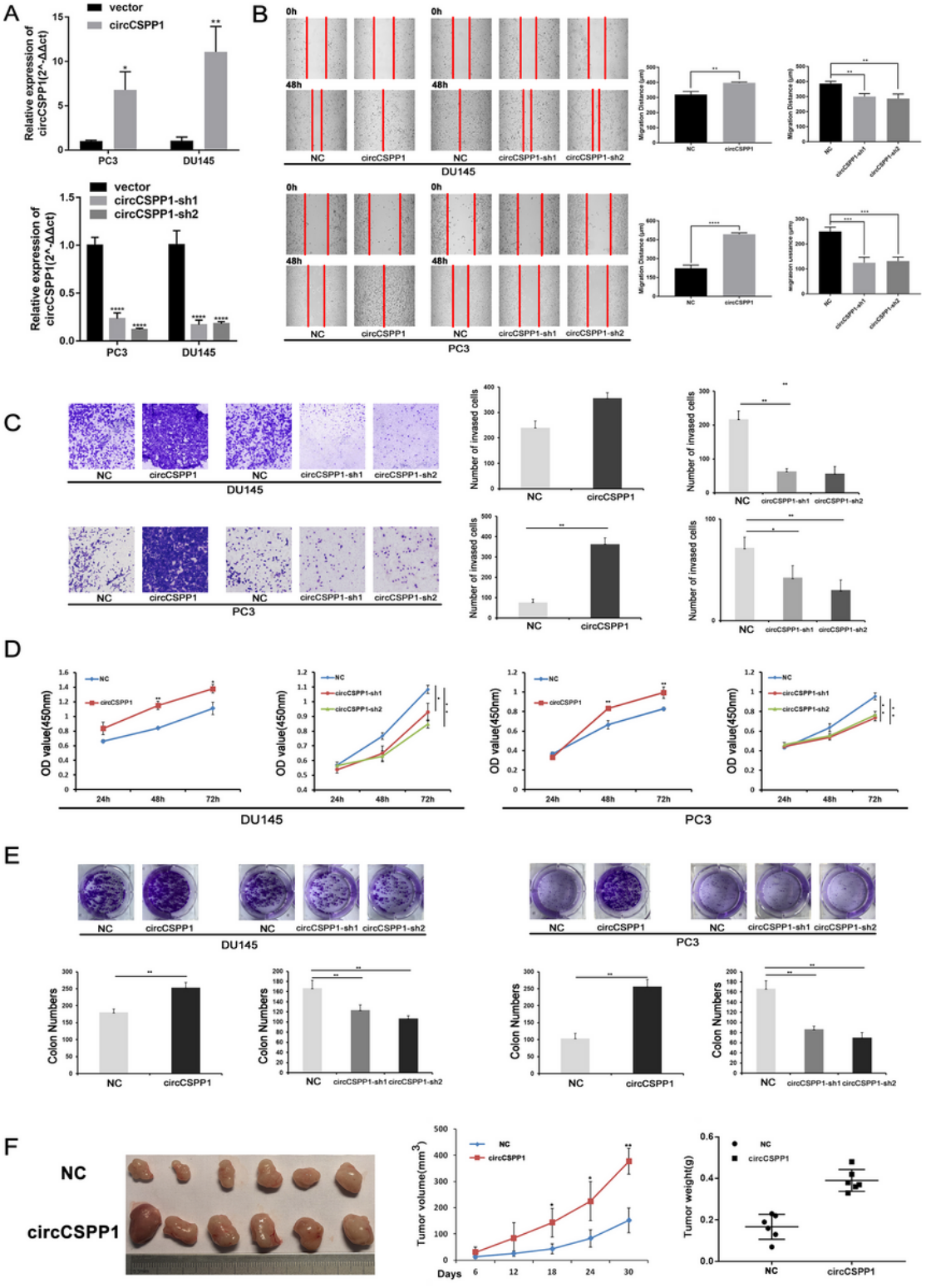

Figure 3

circCSPP1 promotes PCa migration invasion and proliferation in vitro and vivo (A) RT-qPCR for circCSPP1 expression with or without lentivirus overexpression and knockdown PCa cell lines. (B, C) The migration

and invasion capabilities of DU145 and PC3 cells with circCSPP1 overexpression or knockdown was determined through the wound healing and transwell assays. (D, E) The proliferative ability of DU145 and PC3 cells with circCSPP1 overexpression or knockdown was determined through the colony formation and CCK-8 assays. (F) Image of subcutaneous tumors derived from DU145 cell transfected with vector or circCSPP1 in the xenograft model. Tumor volumes were measured every 6 days up to 30 days and the final tumor weight was calculated. Data are shown as means ± SD, Student's t test, ****P<0.0001, ***P<0.001, **P<0.01, *P<0.05.

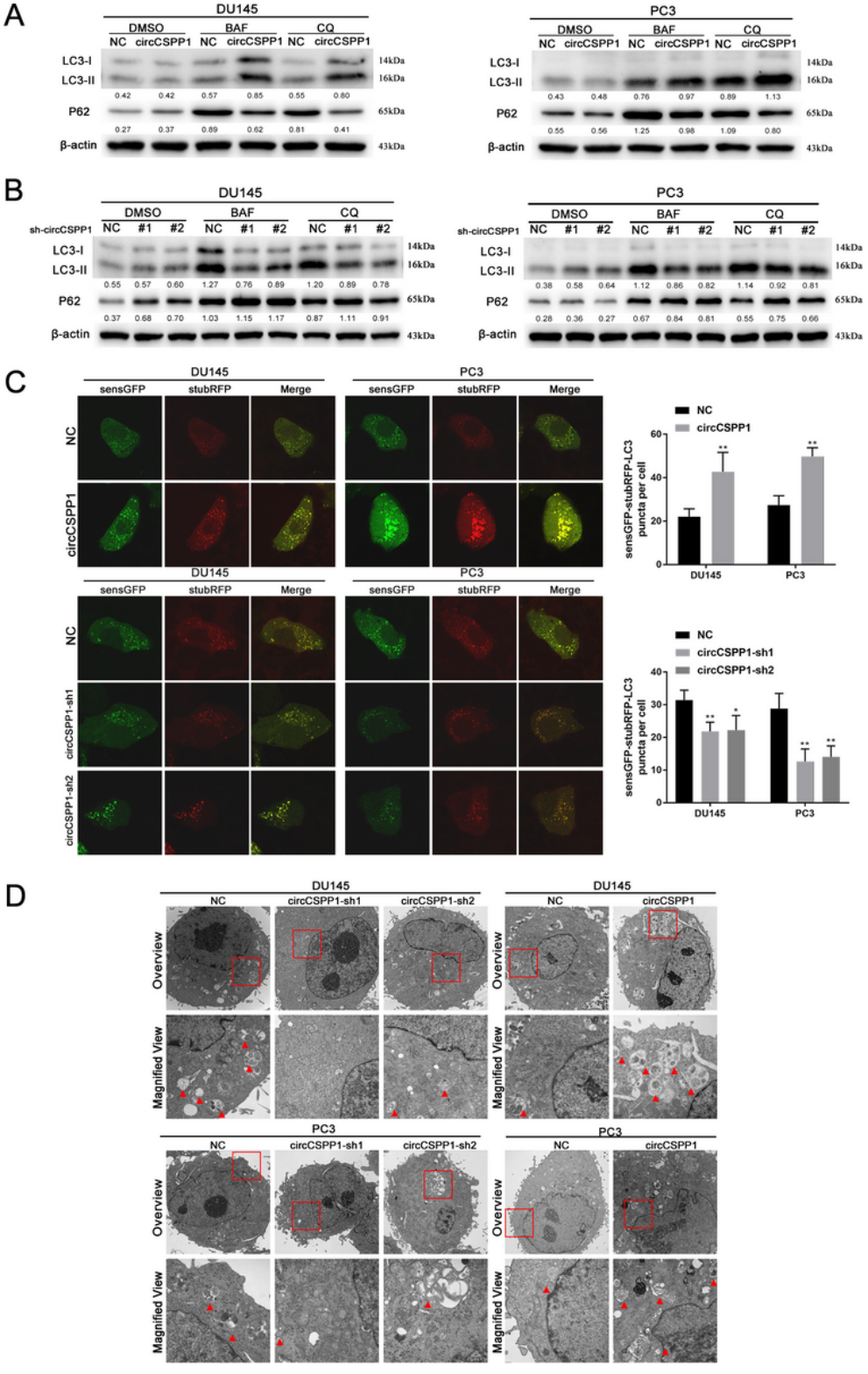

Figure 4

circCSPP1 promotes PCa autophagy in vitro (A) The overexpression of circCSPP1 promotes autophagy in PCa cell lines and the conversions of P62, LC3-II and β-actin under BAF or CQ treatment was detected by western blotting. (B) The knockdown of circCSPP1 attenuates autophagy in PCa cell lines. (C) The overexpression or knockdown of circCSPP1 increases or attenuates the accumulation of LC3-II puncta (green and red overlap). **P<0.01, *P<0.05. (D) Autophagosomes (arrow) observed by transmission electron microscopy (TEM) in circCSPP1 overexpression and knockdown PCa cell lines.

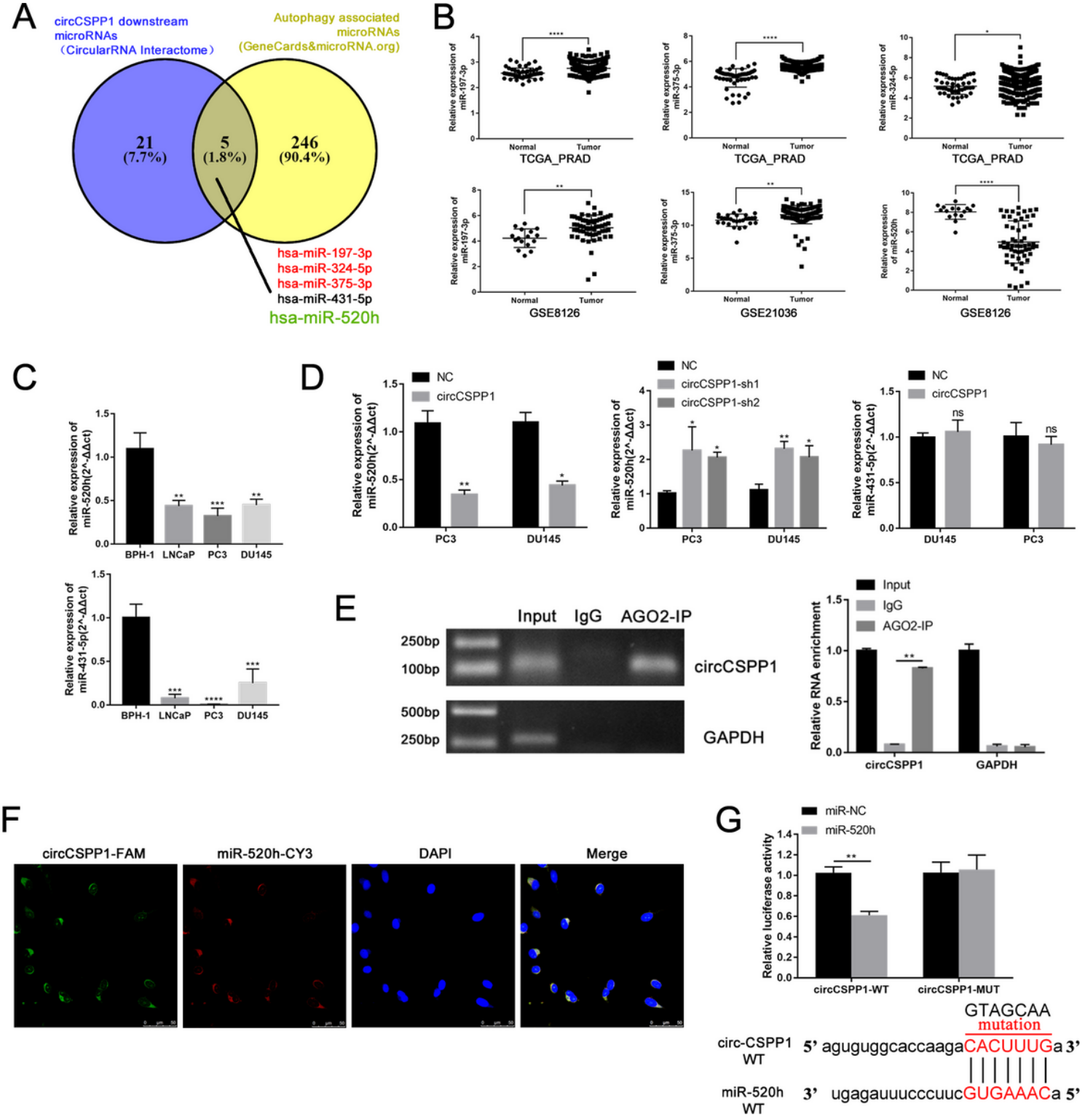

Figure 5

miR-520h is direct target of circCSPP1 in PCa cells (A) Venny diagram shows the putative miRNAs associated with circCSPP1. (B) Differentially expression of putative miRNAs were shown in TCGA database or GEO database, and miR-520h is downregulated in PCa (from GSE:8126) while miR-431-5p was unknown. (C) Native expression of miR-520h and miR-431-5p were detected via RT-qPCR in prostatic cell lines. (D) circCSPP1 is negative correlated with miR-520h in prostatic cell lines except miR-431-5p. (E) AGO2-RNA immunoprecipitation (RIP) assay shows that circCSPP1 could be captured by AGO2 and was determined by agarose gel electrophoresis (AGE). (F) RNA in situ hybridization (FISH) detected the co-localization between circCSPP1 (green) and miR-520h (red) in PC3. (G) The interaction of circCSPP1 with miR-520h sequence was predicted by bioinformatics and the direct target site was confirmed by Luciferase reporter assay. Data are shown as means ± SD, Student's t test, ****P<0.0001, ***P<0.001, **P<0.01, *P<0.05.

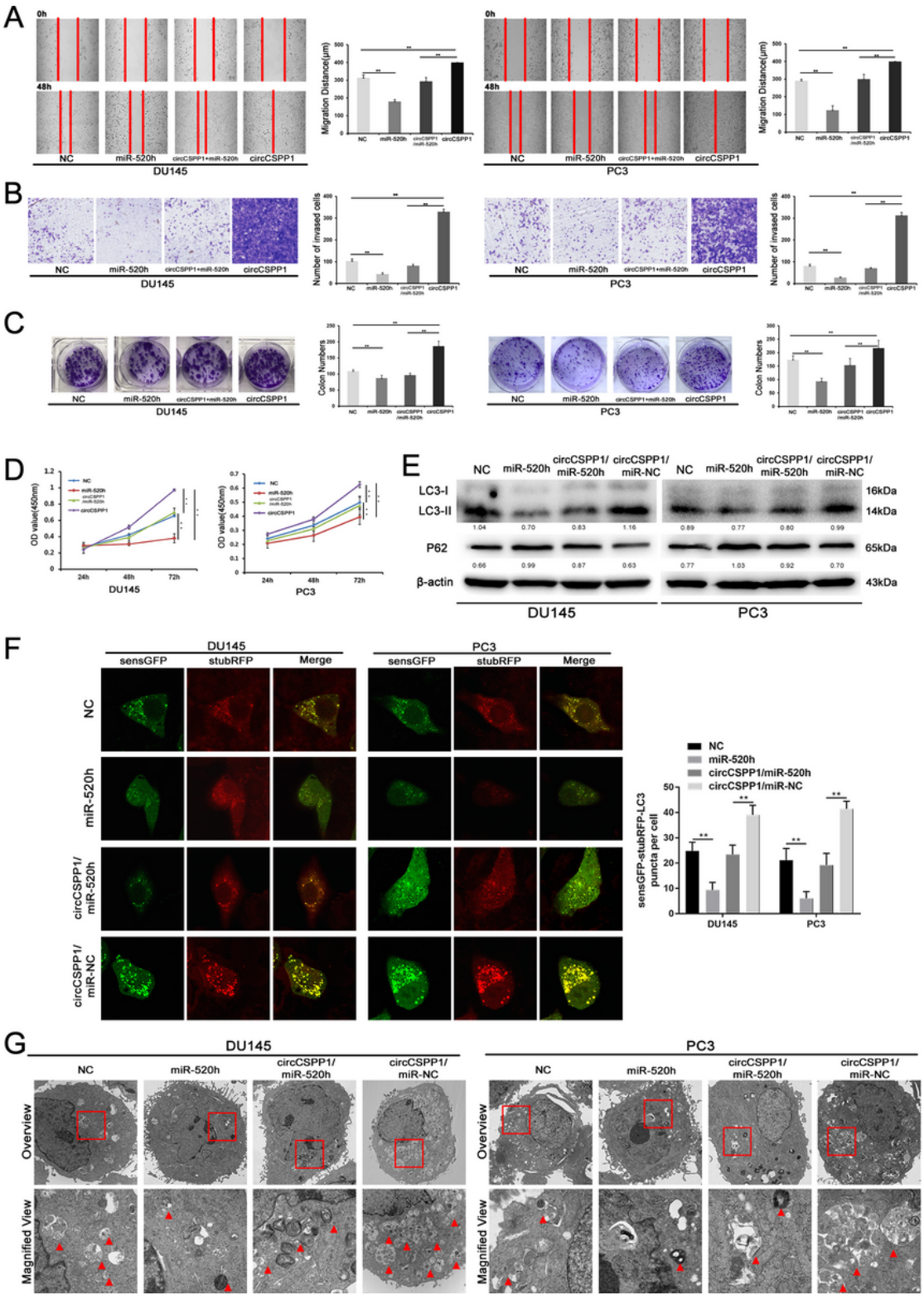

Figure 6

circCSPP1 sponges miR-520h to promote PCa migration, invasion, proliferation and autophagy in vitro (A, B)The migration and invasion capabilities of DU145 and PC3 transfected with lentivirus-circCSPP1 and/or miR-520h mimics were determined with the wound healing and transwell assays. (C, D) The proliferative ability of DU145 and PC3 transfected with lentivirus-circCSPP1 and/or miR-520h mimics was determined through the colony formation and CCK-8 assays. (E) The conversion of P62, LC3-II

normalized to β-actin in DU145 and PC3 transfected with lentivirus-circCSPP1 and/or miR-520h mimics under BAF treatment were detected by western blotting. (F) The accumulation of LC3-II puncta (yellow, green and red overlap) was detected in DU145 and PC3 transfected with circCSPP1 overexpressing lentivirus or miR-520h mimics or co-transfected with both circCSPP1 overexpressing lentivirus and miR-520h mimics. (G) Autophagosomes (arrow) were observed by transmission electron microscopy (TEM) in DU145 and PC3 transfected with lentivirus-circCSPP1 and/or miR-520h mimics. Data are shown as means ± SD, Student's t test, **P<0.01, *P<0.05.

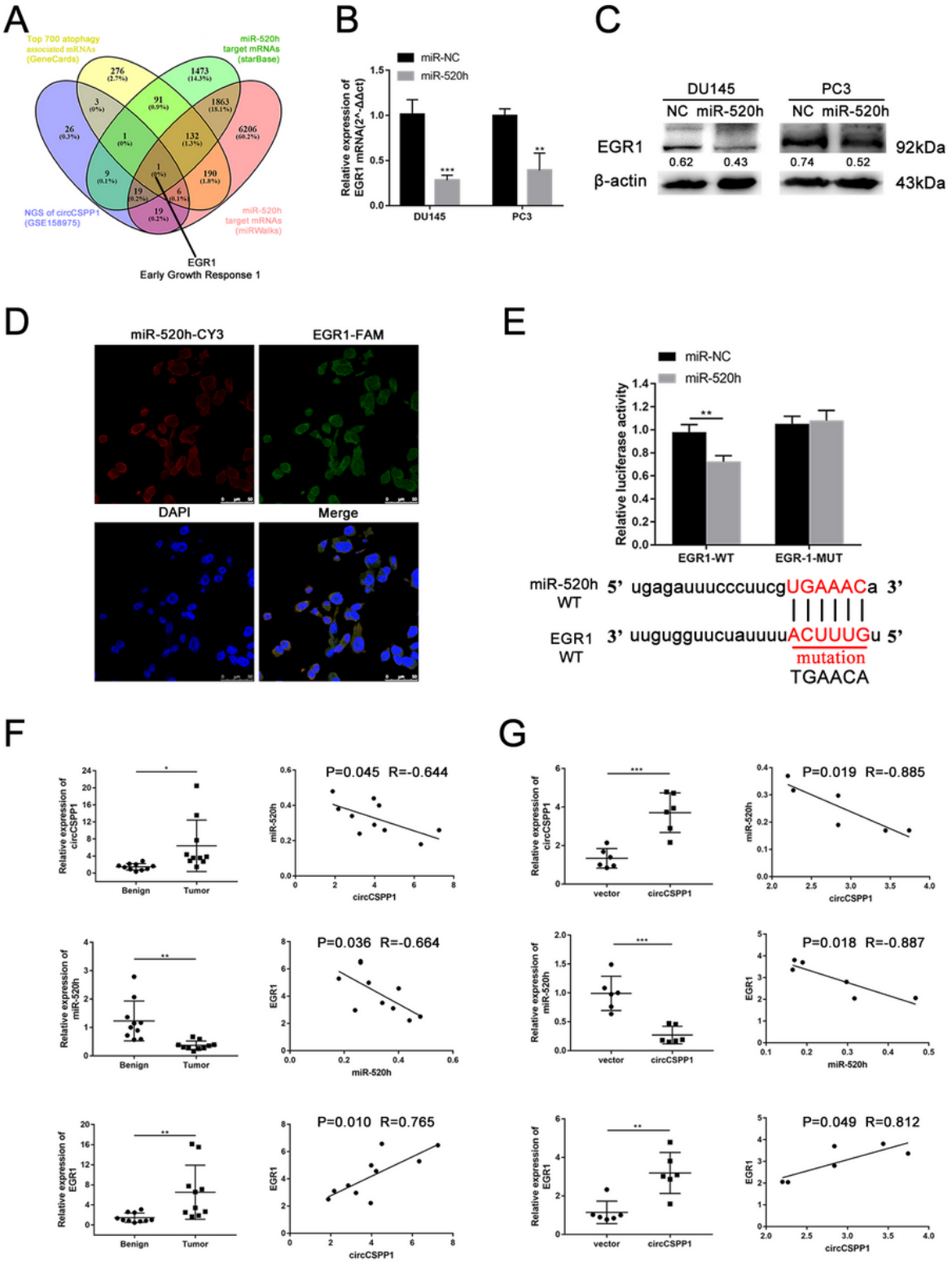

Figure 7

EGR1 is direct target of miR-520h in PCa cells (A) Venny diagram shows EGR1 is the only gene in the overlap. (B) The mRNA expression level of EGR1 was downregulated in DU145 and PC3 transfected with miR-520h mimics. ***P<0.001, **P<0.01. (C) The protein expression level of EGR1 was downregulated in DU145 and PC3 transfected with miR-520h mimics. ***P<0.001, **P<0.01. (D) RNA in situ hybridization detected the co-localization between EGR1 (green) and miR-520h (red) in PC3 cells. (E) The interaction of miR-520 with EGR1 gene sequences was predicted by bioinformatics and Dual-Luciferase reporter assays were performed to confirm their direct target sites. **P<0.01. (F&G) Pattern of the expression of circCSPP1/miR-520h/EGR1 normalized to that of β-actin and the Pearson correlation analysis between any two of three above in 10 pairs of human prostate cancer and benign tissues or 5 pairs of xenograft tumors with vector or circCSPP1 overexpression. Data are shown as means ± SD, Student’s t test, ***P<0.001, **P<0.01, *P<0.05.

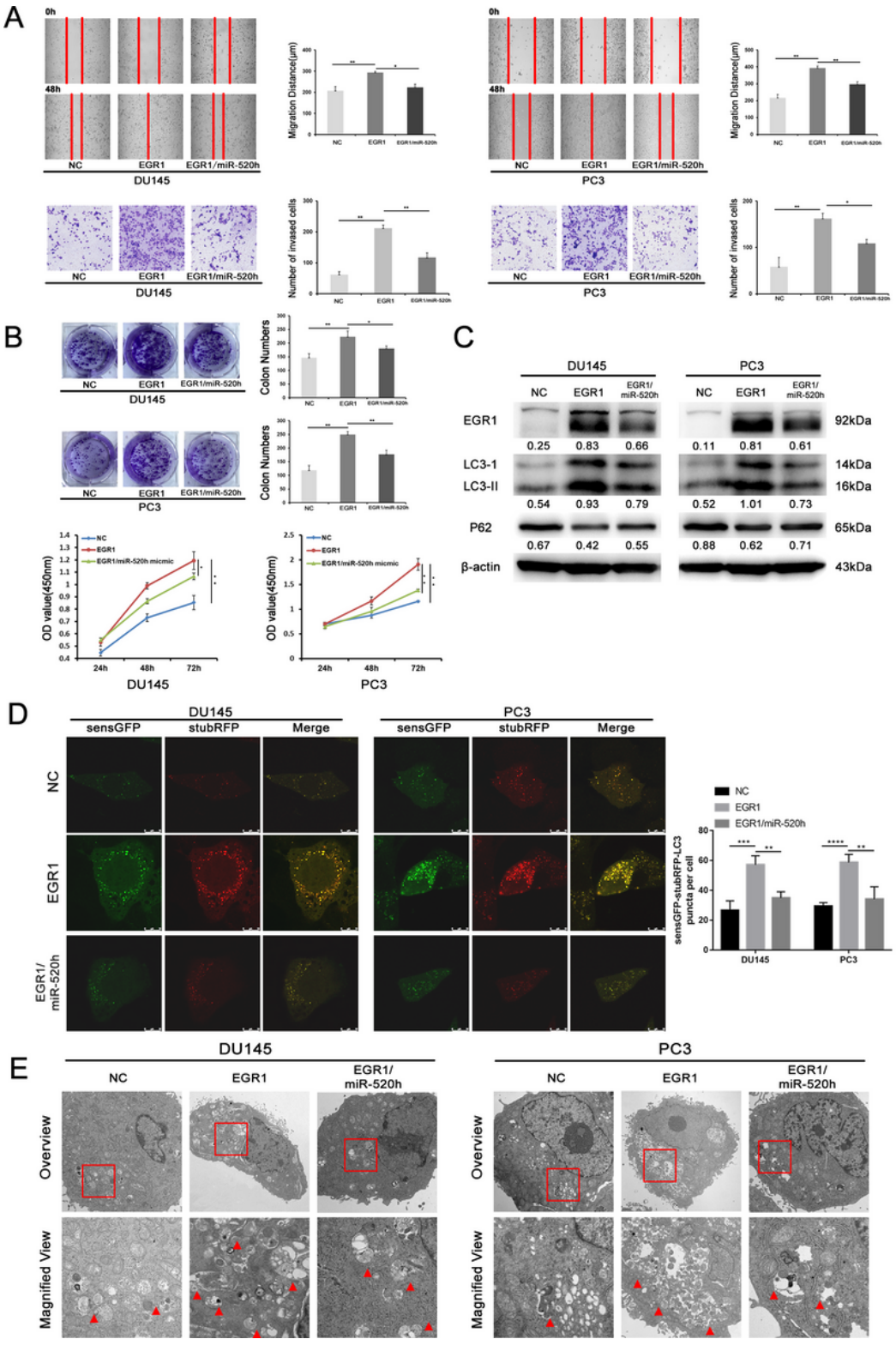

Figure 8

miR-520h silences EGR1 to inhibit PCa migration, invasion, proliferation and autophagy in vitro (A)The migration and invasion capabilities of DU145 and PC3 transfected with pcDNA3.1-EGR1 and/or miR-520h mimics were determined with the wound healing and transwell assays. (B) The proliferative ability of DU145 and PC3 transfected with pcDNA3.1-EGR1 and/or miR-520h mimics was determined through the colony formation and CCK-8 assays. (C) EGR1 expression and the conversion of P62, LC3-II

normalized to β-actin in DU145 and PC3 transfected with pcDNA3.1-EGR1 and/or miR-520h mimics under BAF treament were detected by western blotting.(D) The accumulation of LC3-II puncta (yellow, green and red overlap) was detected in DU145 and PC3 transfected with pcDNA3.1-EGR1 and/or miR-520h mimics. (F) Autophagosomes (arrow) were observed by transmission electron microscopy (TEM) in DU145 and PC3 transfected with pcDNA3.1-EGR1 and/or miR-520h mimics. Data are shown as means ± SD, Student's t test, ****P<0.0001, ***P<0.001, **P<0.01, *P<0.05.

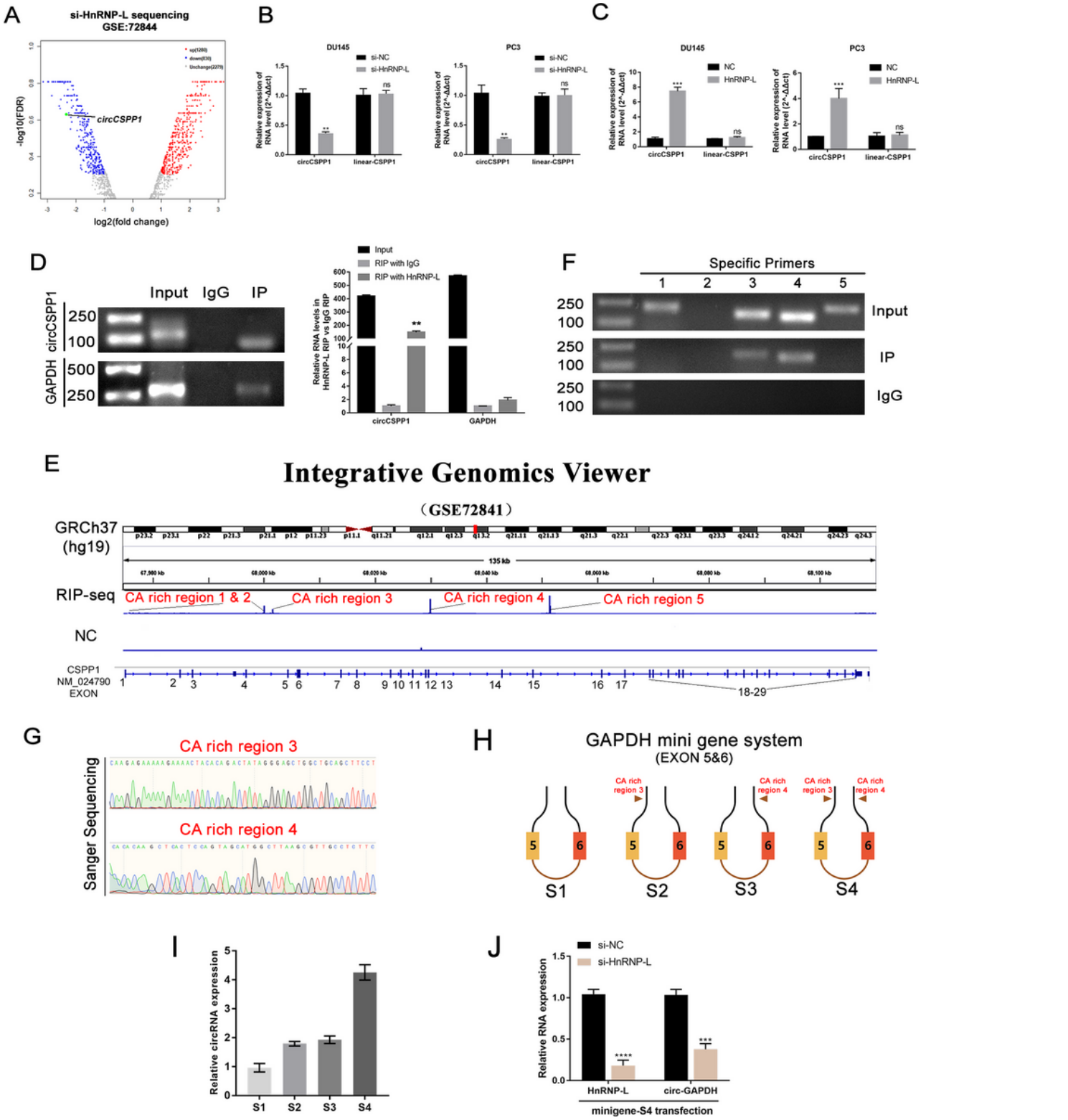

Figure 9

circCSPP1 is upregulated by HnRNP-L (A) The volcano plot shows circCSPP1 was downregulated in LNCaP cell with HnRNP-L downregulation. (B, C) circCSPP1 is positively correlated with HnRNP-L in PCa cell lines via RT-qPCR. Student's t test, ***P<0.001, **P<0.01, ns, not significant. (D) RNA immunoprecipitation (RIP) shows circCSPP1 is binding with HnRNP-L directly, **P<0.01. (E) RIP-sequencing shows the potential binding sites between circCSPP1 with HnRNP-L. (F) RIP-qPCR with specific primers presents that the 3rd and 4th CA repeat sequences of pre-circCSPP1 are the direct binding sites with HnRNP-L.(G) Sanger sequencing confirmed the binding sites in the pre-mRNA of CSPP1 with HnRNP-L. (H) Schematic description showing 4 designed scenarios of GAPDH minigene construction. (I) Relative circRNA expression standardized by pre-mRNA levels in different GAPDH minigenes was analyzed by RT-qPCR. (J) RT-qPCR was performed to evaluate circular GAPDH formation in S4 minigene-transfected cells with the knockdown of HNRNP-L. Student's t test, ****P<0.0001, ***P<0.001.

Supplementary Files

This is a list of supplementary files associated with this preprint. Click to download.

- SupplementaryFigure1.tif
- SupplementaryFigure2.tif
- SupplementaryFigure3.tif
- SupplementaryTable1.docx
- SupplementaryTable2.docx
- SupplementaryTable3.docx